Title
ER phospholipid composition modulates lipogenesis during feeding and in obesity

Journal
Journal of Clinical Investigation, 127(10)

ISSN
0021-9738

Authors
Rong, Xin
Wang, Bo
Palladino, Elisa ND
et al.

Publication Date
2017-10-02

DOI
10.1172/jci93616

Peer reviewed

ER phospholipid composition modulates lipogenesis during feeding and in obesity

Xin Rong,[1] Bo Wang,[1] Elisa N.D. Palladino,[2] Thomas Q. de Aguiar Vallim,[3] David A. Ford,[2] and Peter Tontonoz[1,4,5]

[1]Department of Pathology and Laboratory Medicine, Department of Medicine, UCLA, Los Angeles, California, USA. [2]Department of Biochemistry and Molecular Biology, and Center for Cardiovascular Research, Saint Louis University, St. Louis, Missouri, USA. [3]Division of Cardiology, Department of Medicine, [4]Molecular Biology Institute, and [5]Howard Hughes Medical Institute, UCLA, Los Angeles, California, USA.

Sterol regulatory element–binding protein 1c (SREBP-1c) is a central regulator of lipogenesis whose activity is controlled by proteolytic cleavage. The metabolic factors that affect its processing are incompletely understood. Here, we show that dynamic changes in the acyl chain composition of ER phospholipids affect SREBP-1c maturation in physiology and disease. The abundance of polyunsaturated phosphatidylcholine in liver ER is selectively increased in response to feeding and in the setting of obesity-linked insulin resistance. Exogenous delivery of polyunsaturated phosphatidylcholine to ER accelerated SREBP-1c processing through a mechanism that required an intact SREBP cleavage–activating protein (SCAP) pathway. Furthermore, induction of the phospholipid-remodeling enzyme LPCAT3 in response to liver X receptor (LXR) activation promoted SREBP-1c processing by driving the incorporation of polyunsaturated fatty acids into ER. Conversely, LPCAT3 deficiency increased membrane saturation, reduced nuclear SREBP-1c abundance, and blunted the lipogenic response to feeding, LXR agonist treatment, or obesity-linked insulin resistance. Desaturation of the ER membrane may serve as an auxiliary signal of the fed state that promotes lipid synthesis in response to nutrient availability.

Introduction

Sterol regulatory element–binding protein 1c (SREBP-1c) is a coordinate regulator of gene expression linked to de novo lipogenesis in the liver. Immature SREBP-1c is a transmembrane protein that is retained in the ER through interaction with SREBP cleavage–activating protein (SCAP) and insulin-induced genes (Insigs) (1–3). Under conditions in which lipogenesis is activated, immature SREBP-1c moves to the Golgi, where it is processed by sequential cleavage reactions catalyzed by site 1 and site 2 proteases (4, 5). The mature SREBP-1c transcription factor binds directly to the promoters of a battery of genes involved in the synthesis of fatty acids, including *Fasn*, *Acaca*, and *Scd-1* (6).

The SREBP-1c–dependent lipogenic pathway is stimulated by feeding and is excessively activated in the setting of obesity-linked insulin resistance (6–8). The role of insulin in the transcriptional induction of *Srebf1c* in these contexts is well appreciated. However, the metabolic factors that may serve as signals to permit SREBP-1 processing are incompletely defined. The level of cholesterol in the ER membrane is the key signal controlling the activation of SREBP-2 (9). Loss of SCAP expression inactivates SREBP-1 and SREBP-2 signaling in vivo, indicating that the SCAP/Insig pathway must be involved in the processing of both factors (10). However, unlike SREBP-2 target genes, SREBP-1c targets are not inhibited by elevated hepatic sterol levels (11). This implies that important mechanistic differences exist in the SREBP-1 and SREBP-2 activation pathways that underlie their differential responses to cellular lipids.

SREBP-1c pathway activity is affected by changes in total cellular levels of phospholipids and free fatty acids (12–15). However, the mechanistic role of such factors in SREBP-1c regulation and lipogenesis in vivo is unclear. Prior studies reported that processing of the SREBP ortholog in *Drosophila* S2 cells could be inhibited by saturated phosphatidylethanolamine (PE), but phosphatidylcholine (PC) rather than PE is the major membrane lipid in higher organisms (14). It has also been shown that dramatically reducing the total cellular phospholipid levels activates SREBP-1 processing by disrupting COPII-dependent ER-Golgi transport and causing the mislocalization of site 1 protease (S1P) and S2P to ER (15). The possibility that individual phospholipids might differentially influence SREBP processing based on their acyl chain composition has not been explored.

Liver X receptors (LXRs) are important modulators of hepatic lipogenesis, due in part to their ability to regulate the SREBP-1c pathway at the level of transcription (16, 17). LXRs also mediate induction of *Srebf1c* mRNA in response to increased hepatic sterol levels (11). Treatment of mice with a synthetic LXR agonist promotes hepatic triglyceride synthesis, stimulates VLDL secretion, and raises plasma triglyceride levels (18, 19). Conversely, SREBP-1c expression and lipogenesis are severely reduced in mice lacking LXRα and LXRβ (16, 20). Loss of LXRs in *ob/ob* mice reverses the fatty liver phenotype characteristic of systemic insulin resistance (20).

The effects of LXRs on SREBP-1c activity have heretofore been presumed to be due entirely to their effects on *Srebf1c* transcription. We found that LXRs modulate SREBP-1c processing independently of transcription through induction of the phospholipid-remodeling enzyme LPCAT3. These findings led to the recognition that specific ER phospholipids, particularly linoleoyl and arachidonoyl PC, are stimulators of SREBP-1c maturation whose levels are regulated during feeding and in obesity. Accordingly, LPCAT3-

Conflict of interest: The authors have declared that no conflict of interest exists.
Submitted: March 2, 2017; **Accepted:** July 11, 2017.
Reference information: *J Clin Invest*. 2017;127(10):3640–3651.
https://doi.org/10.1172/JCI93616.

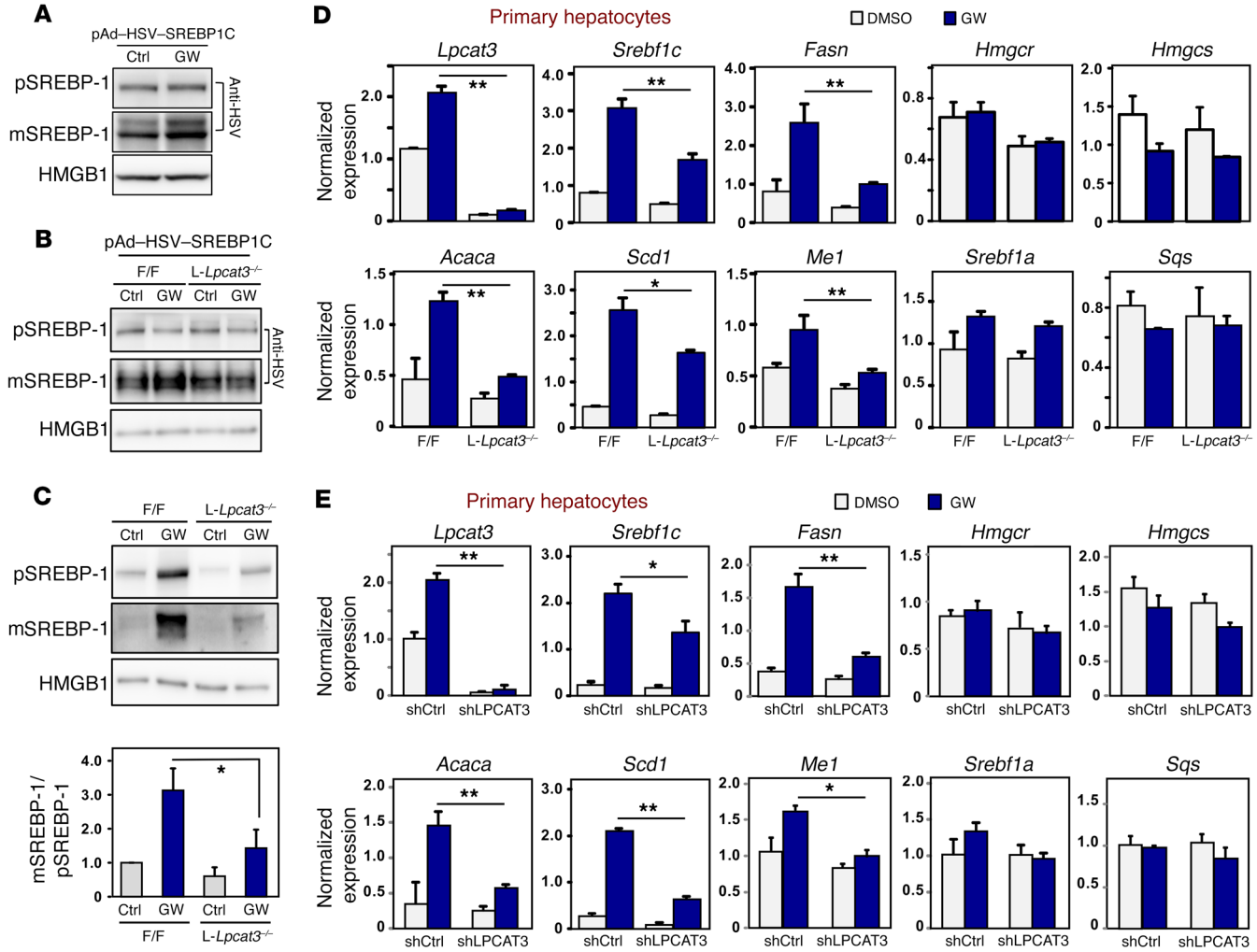

Figure 1. The Lxr/LPCAT3 pathway regulates SREBP-1c processing in hepatocytes. (**A**) Primary mouse hepatocytes from C57BL/6 mice were infected with adenovirus expressing HSV-tagged SREBP-1c for 36 hours and treated with GW3965 (GW, 1 μM) for the last 24 hours. SREBP-1c from membrane fraction (precleaved SREBP-1 [pSREBP-1]) and nuclear fraction (mature SREBP-1 [mSREBP-1]) were analyzed by immunoblotting with anti-HSV antibody. HMGB1 served as internal loading controls for nuclear fractions. (**B**) Primary mouse hepatocytes from *Lpcat3*$^{fl/fl}$ (F/F) and *Lpcat3*$^{fl/fl}$ albumin-Cre^{+} (L-*Lpcat3*$^{-/-}$) mice were infected with adenovirus expressing HSV-tagged SREBP-1c for 36 hours and treated with GW3965 for the last 24 hours. SREBP-1c from membrane fraction (pSREBP-1) and nuclear fraction (mSREBP-1) was analyzed by immunoblotting with anti-HSV antibody. (**C**) Primary mouse hepatocytes from *Lpcat3*$^{fl/fl}$ (F/F) and *Lpcat3*$^{fl/fl}$ albumin-Cre^{+} (L-*Lpcat3*$^{-/-}$) mice were treated with DMSO (veh) or GW3965 (1 μM) for 24 hours. Endogenous SREBP-1 from membrane and nuclear fractions was analyzed by immunoblotting (upper panel) and quantified by ImageJ. The ratio of mSREBP-1 to pSREBP-1 was shown (lower panel). HMGB1 served as an internal loading control for the nuclear fraction. (**D**) Gene expression in primary hepatocytes treated as in **C** was analyzed by real-time PCR. (**E**) Primary mouse hepatocytes from C57BL/6 mice were infected with adenoviral shRNA vectors targeting LPCAT3 (shLPCAT3) or control (shCtrl) for 36 hours and treated with GW3965 (1 M) for the last 24 hours. Gene expression was analyzed by real-time PCR. $^{*}P < 0.05$; $^{**}P < 0.01$. Values are shown as mean ± SD.

dependent incorporation of these lipids into membranes is required for optimal homeostatic regulation of lipogenesis in vivo. These results highlight a mechanism whereby membrane phospholipid remodeling differentially affects the maturation of SREBP-1c and SREBP-2 in physiology and in the setting of metabolic disease.

Results

LXRs promote SREBP-1c cleavage through LPCAT3 induction. The observation that LXR agonists appeared to have effects on the SREBP-1c pathway that were disproportionate to their effects on *Srebf1c* mRNA levels (16, 21) led us to explore whether additional mechanisms of regulation might be involved. We first established a cell system in which immature full-length, Hsv-tagged SREBP-1c was expressed from a viral promoter. This allowed us to uncouple effects of LXR on *Srebf1c* transcription from potential effects on posttranscriptional processes. Remarkably, treatment of Hsv-SREBP-1c–expressing primary mouse hepatocytes with the synthetic LXR agonist GW3965 for 24 hours led to increased abundance of tagged nuclear SREBP-1c (Figure 1A).

We hypothesized that the apparent ability of the LXR ligand to promote SREBP-1c processing was likely mediated by the induction of one or more LXR target genes. *Lpcat3* was an attractive candidate mediator of this effect, since it is known to be involved in ER membrane lipid remodeling (19, 22). We therefore compared

the ability of LXR agonist to promote the cleavage of exogenously expressed Hsv–SREBP-1c in primary hepatocytes isolated from floxed control mice with that in liver-specific LPCAT3-deficient (*Lpcat3*$^{fl/fl}$ albumin-Cre, hereafter referred to as L-*Lpcat3*$^{-/-}$) mice (19). We found that loss of LPCAT3 expression completely blocked the ability of LXR agonist to increase tagged nuclear SREBP-1c protein levels (Figure 1B). Moreover, the ability of LXR agonist to increase the abundance of *endogenous* mature nuclear SREBP-1c was also markedly diminished in the absence of LPCAT3 (Figure 1C). Consistent with this finding, the effect of LXR agonist treatment on the expression of lipogenic genes, such as *Fasn*, *Scd-1*, and *Acc-1*, was also strongly reduced in LPCAT3-deficient primary hepatocytes (Figure 1D).

To exclude the possibility that the defect in lipogenic gene expression observed in LPCAT3-deficient hepatocytes was secondary to chronic metabolic changes in L-*Lpcat3*$^{-/-}$ mice, we conducted parallel experiments in WT primary hepatocytes transduced with control or LPCAT3-specific adenoviral shRNA vectors (22). These experiments showed that acute loss of LPCAT3 expression also compromised the lipogenic response to LXR agonist treatment (Figure 1E). Interestingly, the effects of LPCAT3 inhibition were selective for SREBP-1c target genes. There was no effect of loss of LPCAT3 on the expression of canonical SREBP-2 target genes, including *Hmgcr*, *Hmgcs*, and *Sqs* (Figure 1, D and E).

LPCAT3 expression is required for optimal lipogenesis in mouse liver. To explore the potential contribution of LXR-dependent LPCAT3 regulation to SREBP-1 processing and lipogenesis in vivo, we employed loss-of-function mouse models. We first assessed the effect of chronic loss of LPCAT3 expression in mouse liver. Floxed control or L-*Lpcat3*$^{-/-}$ mice were treated for 3 days with 40 mpk GW3965 and lipogenic gene expression was assessed. Interestingly, the lipogenic effect of LXR agonist was blunted in the absence of LPCAT3 expression (Figure 2A). Furthermore, this reduction in lipogenic gene expression was associated with reduced levels of nuclear SREBP-1c protein in L-*Lpcat3*$^{-/-}$ mice (Figure 2B). To exclude the possibility that the defects in lipogenic gene expression observed in LPCAT3-deficient mice were secondary to chronic metabolic changes, we also tested the consequences of acute suppression of hepatic *Lpcat3* expression in vivo. C57BL/6 mice transduced with an LPCAT3-specific shRNA adenoviral vector showed reduced expression of a battery of lipogenic genes following LXR agonist treatment compared with mice transduced with shRNA adenoviral control (Figure 2C). Consistent with the results of our in vitro studies, there was no effect of loss of LPCAT3 on the expression of SREBP-2 target genes, including *Hmgcr*, *Sqs*, and *Hmgcs*. Thus, both acute and chronic LPCAT3 deficiency compromised the lipogenic response to LXR agonism, strongly suggesting that LPCAT3 activity is mechanistically linked to SREBP-1c pathway activation. Importantly, we observed no effect of LXR agonist on the stability of exogenously expressed mature nuclear SREBP-1c (Figure 2, D and E), implicating reduced production of the nuclear form rather than accelerated turnover as the basis for the LXR-LPCAT3 effects.

PC acyl chain composition regulates the processing of SREBP-1c. We hypothesized that the ability of LXR and LPCAT3 to increase the abundance of polyunsaturated PC species, particularly arachidonate and linoleate, in the ER might explain their effects on SREBP-1c processing. The impact of selectively altering membrane phospholipid acyl chain composition on SREBP processing in mammalian cells has not previously been addressed. We tested the ability of exogenous phospholipids to affect the processing of Hsv-tagged SREBP-1c in primary hepatocytes. In one set of experiments, we delivered phospholipids to cells using liposomes with a composition closely matching that of ER (23). Prior studies reported that this liposome vehicle (which contains a mixture of PC, PE, phosphatidylserine [PS], and phosphatidylinositol [PI]) delivers phospholipids to ER (23), and we confirmed its ability to deliver fluorescently labeled PC to intracellular membranes of primary hepatocytes by microscopy (Figure 3A). We observed delivery of saturated and polyunsaturated PC species to cells with this phospholipid (PL) vehicle (Figure 3B). We adjusted the composition of this vehicle such that the PC component was contributed by a single species and tested how increasing or decreasing acyl chain saturation influenced SREBP-1c processing. Treatment with liposomes containing PC with polyunsaturated chains (18:0/18:2 PC and 18:0/20:4 PC) led to increased nuclear SREBP-1 abundance compared with those containing unsaturated or monounsaturated chains (Figure 3, C and D). Lipidomics analysis of the liposome-treated cells confirmed that the intracellular PC species changed in response to the specific liposome treatment (Supplemental Figure 1; supplemental material available online with this article; https://doi.org/10.1172/JCI93616DS1). We note that all of the liposomes modestly increased nuclear SREBP-1c levels compared with treatment with saline vehicle alone. This baseline effect could also possibly be due to changes in ER saturation, since the bovine and porcine tissue–derived PE, PI, and PS components of the liposomes contained a mixture of both saturated and unsaturated chains. Nevertheless, manipulating the acyl chain saturation of the PC component in these liposomes clearly affected SREBP-1c maturation.

As a complementary approach, and to eliminate the contribution of carrier liposomes to cellular phospholipids, we incubated primary hepatocytes with liposomes composed entirely of saturated, monounsaturated, or polyunsaturated PC. In agreement with our results with complex liposome vehicles, polyunsaturated arachidonoyl PC promoted processing (Figure 3E), whereas monounsaturated PC had no effect. Interestingly, saturated PC inhibited SREBP-1c processing compared with saline control in these experiments.

We hypothesized that decreasing ER membrane saturation was promoting the movement of the SREBP-1c/SCAP complex from the ER to the Golgi for processing. If this model is correct, then the effects of the LXR/LPCAT3 pathway on SREBP-1 processing should be dependent on SCAP expression. We isolated primary hepatocytes from floxed-SCAP mice and transduced them in vitro with adenoviral vectors expressing GFP control or Cre recombinase. We found that the effects of LXR activation on nuclear SREBP-1c accumulation were lost in primary hepatocytes lacking SCAP (Figure 3F). Previous studies have shown that brefeldin A causes the relocation of site-1 and site-2 proteases from Golgi to ER, resulting in SCAP-independent cleavage (24). We found that the inhibitory effect of LPCAT3 deficiency was lost in the setting of brefeldin A treatment (Supplemental Figure 2), consistent with the hypothesis that LPCAT3 may act by enhancing translocation of the SCAP/ SREBP complex from ER to Golgi.

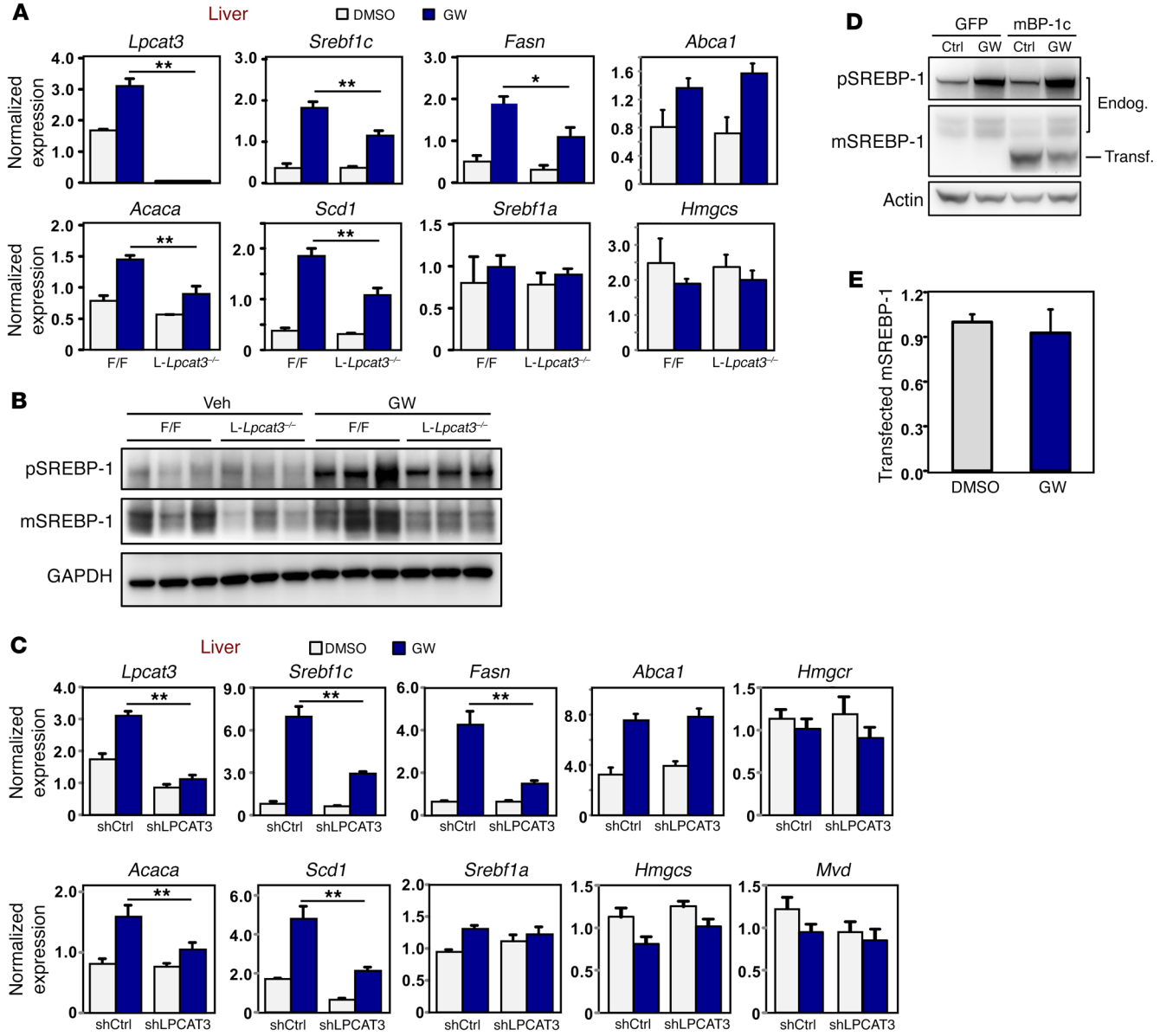

Figure 2. The LXR/LPCAT3 pathway regulates SREBP-1c processing in mouse liver. (**A**) *Lpcat3*$^{fl/fl}$ (F/F) and *Lpcat3*$^{fl/fl}$ albumin-Cre^{+} (L-*Lpcat3*$^{-/-}$) mice were gavaged with GW3965 at 40 mg/kg body weight once per day for 3 days. Liver gene expression was analyzed by real-time PCR. n = 5 per group. (**B**) *Lpcat3*$^{fl/fl}$ (F/F) and *Lpcat3*$^{fl/fl}$ albumin-Cre^{+} (L-*Lpcat3*$^{-/-}$) mice were gavaged with GW3965 at 40 mg/kg body weight once per day for 3 days. Liver protein was analyzed by immunoblotting. n = 3 per group. (**C**) C57BL/6 mice were transduced with adenoviral shLPCAT3 or shCtrl vectors for 8 days and gavaged with GW3965 at 40 mg/kg body weight once per day on days 6, 7, and 8. Liver gene expression was analyzed by real-time PCR. n = 5 per group. Statistical analysis was by 2-way ANOVA with Bonferroni's post hoc tests. The post hoc test results between shCtrl and shLPCAT3 in GW3965-treated groups are shown in the figure. (**D**) 293T cells were transfected with plasmids expressing GFP control or truncated nuclear form of SREBP-1c and treated with GW3965 at 1 μM as described in Methods. Total cell lysate was analyzed by immunoblotting with anti–SREBP-1 antibody. (**E**) Immunoblotting results of transfected truncated nuclear SREBP-1c from **D** were quantified from 4 independent experiments by ImageJ. Statistical analysis was by Student's t test. $^{*}P < 0.05$; $^{**}P < 0.01$. Values are shown as mean ± SEM.

These observations indicate that the effects of LXR and LPCAT3 on SREBP-1c maturation require an intact SCAP pathway.

Dynamic regulation of ER PC composition during feeding. We next asked whether endogenous polyunsaturated PC levels were altered in physiologic settings where hepatic lipogenesis is active. Fasting and then refeeding mice is known to robustly activate the SREBP-1c pathway and to stimulate lipogenesis (21). We isolated ER membranes by density gradient centrifugation from livers of C57BL/6 mice that had been fasted for 12 hours and then refed with a carbohydrate-rich diet as described (21). The enrichment of ER membranes in these preparations was confirmed by immunoblotting with cellular compartment markers (Figure 4A). Global analysis of phospholipids by electrospray ionization–tandem mass spectrometry (ESI-MS/MS) revealed striking changes in a range of individual PC species in these experiments. The abundance of polyunsaturated PCs, including 18:0/18:2 PC, 18:1/18:2 PC, 18:0/20:4 PC,

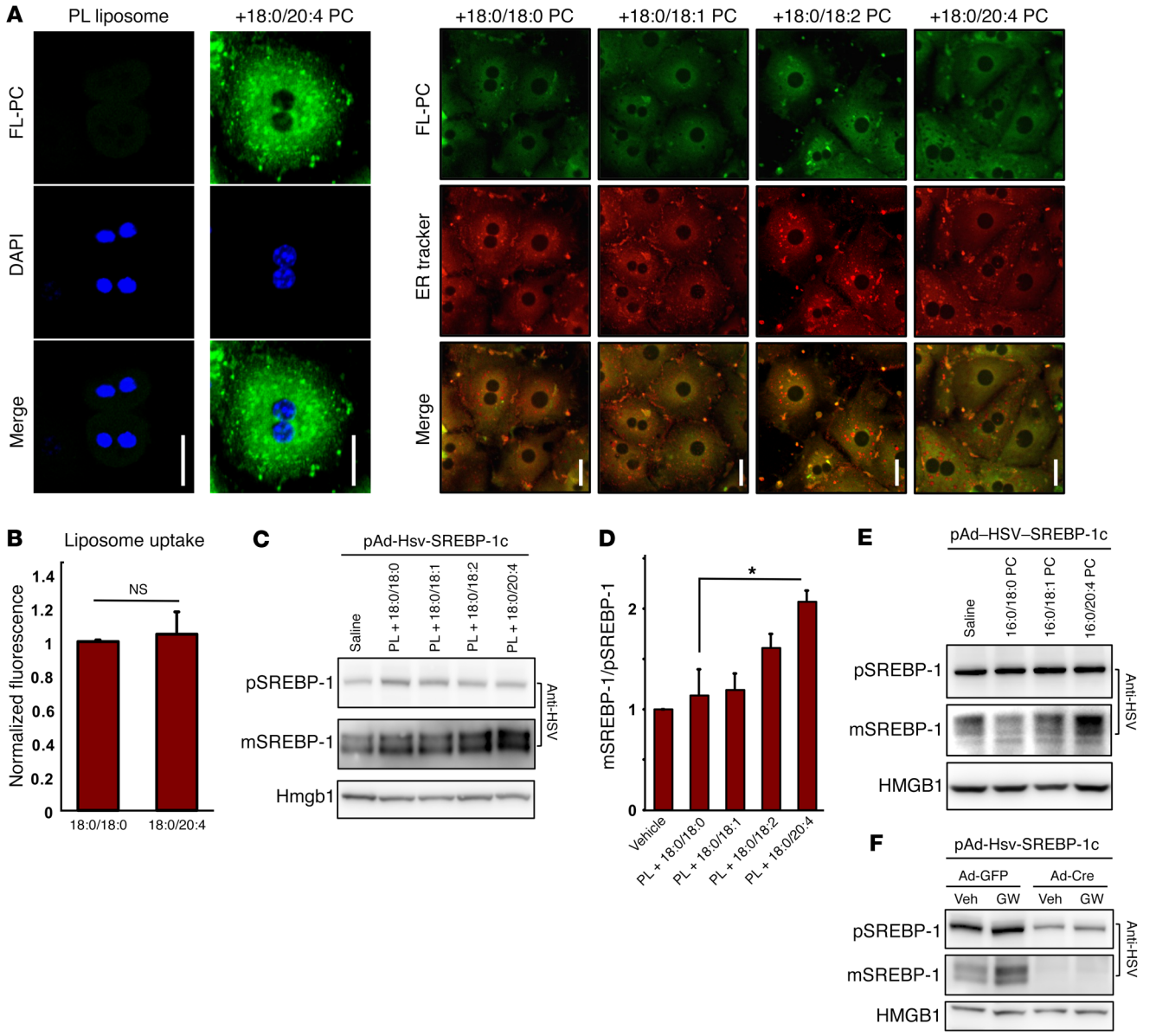

Figure 3. PC acyl chain composition regulates SREBP-1c processing. (**A**) Analysis of intracellular distribution fluorescently labeled PC following administration of ER-targeting liposomes. Fluorescently labeled ER-targeting liposomes enriched for different PC species were formulated as described in Methods. The PE, PS, and PI components were identical between liposomes, and the PC component was contributed by defined species as indicated. Liposomes were labeled with 1% bodipy-conjugated PC (green). DAPI (blue, left panels) and ER tracker (red, right panels) were used for costaining. Scale bars: 20 μm. (**B**) Quantification of ER-targeting liposome uptake. Cells were treated with fluorescently labeled carrier liposome enriched for either 18:0/18:0 PC or 18:0/20:4 PC for 1 hour. Cells were washed with PBS and lysed in RIPA buffer and fluorescence was measured with a plate reader. (**C**) Primary hepatocytes from C57BL/6 mice were infected with adenovirus expressing HSV–tagged SREBP-1c for 24 hours and treated with the indicated ER-targeting liposome (30 μM total phospholipid concentration) for the last 3.5 hours. Membrane and nuclear fractions were isolated and analyzed by immunoblotting. (**D**) Quantification of Western blot results from 3 independent experiments shown in part **C**. *$P < 0.05$, Student's t test. (**E**) Primary hepatocytes from C57BL/6 mice were infected with adenovirus expressing HSV-tagged SREBP-1c for 24 hours and treated with liposomes composed of the indicated single PC species at 30 μM for the last 3.5 hours. Membrane and nuclear fractions were isolated and analyzed by immunoblotting. (**F**) Primary hepatocytes from *Scap*$^{fl/fl}$ mice were infected with adenoviral GFP or Cre recombinase and treated with GW3965 (1 μM) for 24 hours. Protein from total cell lysates was analyzed by immunoblotting.

18:1/20:4 PC, and 18:0/22:6 PC, was increased in refed compared with fasted mice (Figure 4B). Several monounsaturated PC species were also increased, particularly 16:0/18:1 PC. As expected, PE was far less abundant than PC in ER membranes and, with the exception of a decrease in 16:0/18:2 PE, only modest changes in acyl chain saturation were observed in response to feeding (Supplemental Figure 4A). Similar analyses conducted on mice refed with a high-fat diet (60% fat by calorie) revealed increased abundance of primarily 18:2- and 20:4-containing PC species (Figure 4C). In contrast with the high-carbohydrate diet, there was no increase in 16:0/18:1 PC on a high-fat diet, likely reflecting a difference in the proportion of PL acyl chains derived from de novo fatty acid synthesis in the 2 set-

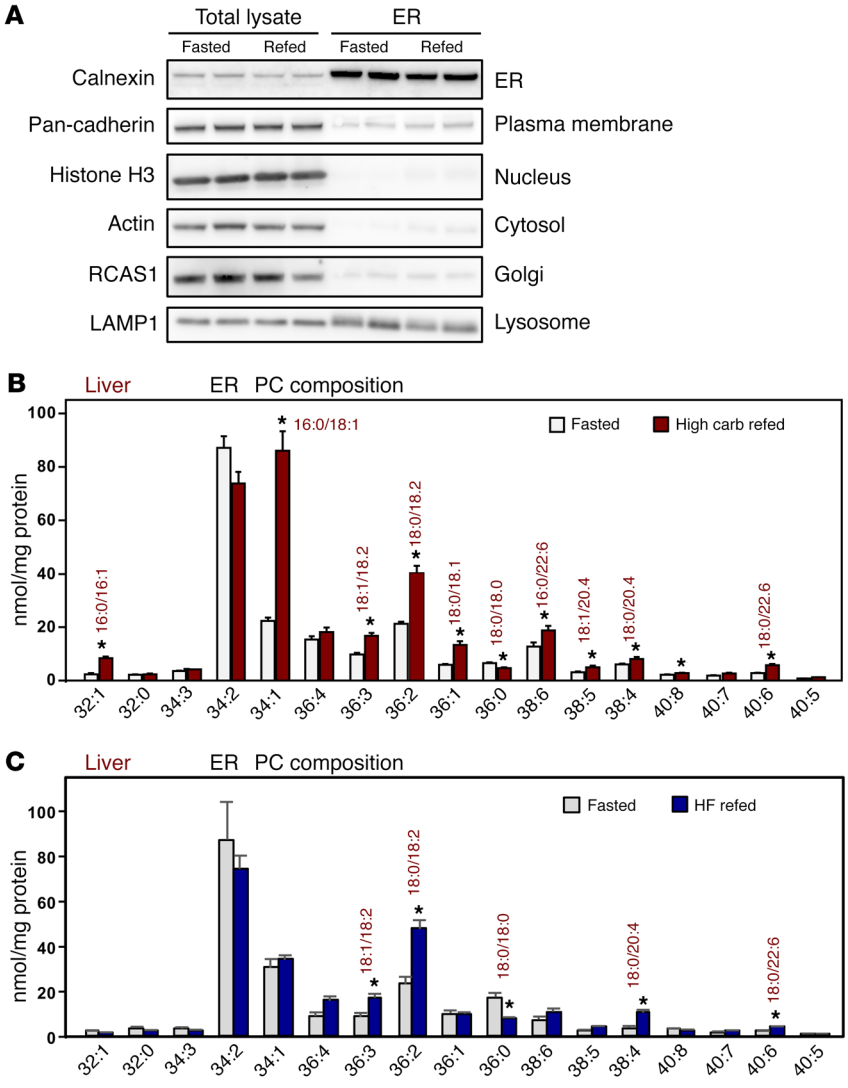

Figure 4. Liver ER membrane composition is dynamically regulated during feeding. (**A**) Validation of ER fractionation of mouse liver extracts by immunoblot analysis of subcellular markers. (**B**) ESI-MS/MS analysis of PC species in the ER fraction from livers of C57BL/6 mice fasted 12 hours or fasted 12 hours and refed 12 hours with a high-carbohydrate diet (21). Indicated (*sn*-1/*sn*-2) molecular species were confirmed by product ion scanning for aliphatic composition. $n = 6$ per group. Statistical analysis was by Student's t test with correction for multiple comparisons using the Holm-Šidák method. $^*P < 0.05$. Values are shown as mean ± SEM. (**C**) ESI-MS/MS analysis of PC species in the ER fraction from livers of C57BL/6 mice fasted 12 hours or fasted 12 hours and refed 12 hours with a high-fat diet (60% fat). Indicated (*sn*-1/*sn*-2) molecular species were confirmed by product ion scanning for aliphatic composition. $n = 6$ per group. Statistical analysis was by Student's t test with correction for multiple comparisons using the Holm-Šidák method. $^*P < 0.05$. Values are shown as mean ± SEM.

tings. Major choline glycerophospholipid molecular species identified in ER were subjected to further analyses to provide information for the regioisomers of acyl chains, as described in Methods. The sodiated adducts of major species were subjected to collisional-activated dissociation (CAD) analyses, which yields regioisomer information by determining the ratio of the fragment ions from the loss of trimethylamine and the fatty acid of the parent molecular ion. These analyses confirmed assignments of saturated fatty acyl chains to the sn-1 position and unsaturated fatty acyl chains to the sn-2 position. These analyses further revealed that regioisomers were largely unchanged between fasting and high-fat diet refeeding (Supplemental Figure 3). The relative abundance of regioisomers of 16:0/20:4 PC was slightly altered between the 2 conditions. Collectively, these results demonstrate that the ER phospholipid composition is substantially altered in the fed state, with the net change being a decrease in sn-2 PC acyl chain saturation.

To determine the requirement of LPCAT3 enzyme activity in facilitating the change in ER PC composition during feeding, we repeated our ER isolation and PL analysis in livers of L L-*Lpcat3*$^{-/-}$ mice. As expected, loss of LPCAT3 did not alter the abundance of monounsaturated species during feeding, consistent with prior work showing that LPCAT3 is not required for incorporation of 18:1 into membranes (19). However, the change in abundance of the majority of polyunsaturated PC species, particularly the most abundant 18:2-containing PC species, was reduced in the absence of LPCAT3 (Supplemental Figure 4B). We speculate that the residual 20:4-containing PC species observed in L-*Lpcat3*–KO samples is likely to reflect the contribution of nonparenchymal cells (which do not express Cre and retain LPCAT3 expression) to total liver ER (19).

To test the hypothesis that LPCAT3-dependent incorporation of polyunsaturated PC into ER membranes is important for the lipogenic response to feeding, we performed fasting-refeeding studies on control and L-*Lpcat3*$^{-/-}$ mice. The induction of SREBP-1c target genes in response to feeding was blunted in mice deficient in hepatic LPCAT3 (Figure 5A). Furthermore, this defect correlated with reduced mature nuclear SREBP-1c protein in livers of L-*Lpcat3*$^{-/-}$ mice (Figure 5B). We also assessed the requirement for LPCAT3 expression for the lipogenic response to insulin. Consistent with the results of the fasting-refeeding studies, loss of hepatic LPCAT3 expression blunted the induction of *Fasn* in response to insulin bolus (Figure 5C).

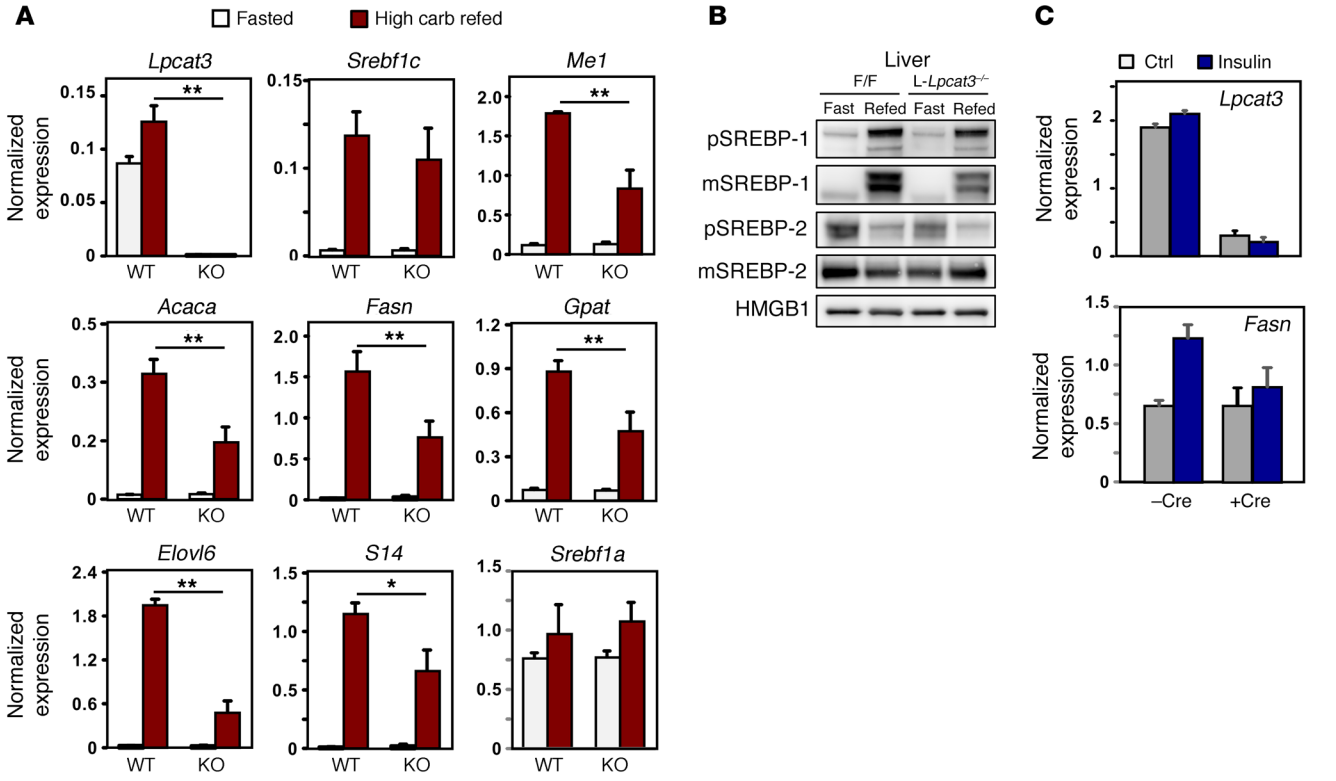

Figure 5. LPCAT3 modulates the lipogenic response to feeding. (**A**) *Lpcat3*$^{fl/fl}$ (F/F) and *Lpcat3*$^{fl/fl}$ albumin-Cre^{+} (L-*Lpcat3*$^{-/-}$) mice were fasted 12 hours or fasted 12 hours and refed 12 hours with a high-carbohydrate diet. Gene expression was analyzed by real-time PCR. n = 6 per group. Statistical analysis was by 2-way ANOVA with Bonferroni's post hoc tests. (**B**) Membrane and nuclear fractions were prepared from fresh livers from mice treated as in **A**. Samples of 4 mice from each condition were pooled for measurement of endogenous SREBP-1 and SREBP-2 protein. (**C**) *Lpcat3*$^{fl/fl}$ mice were transduced with adenoviral vector control or adenoviral-Cre for 7 days and then administered vehicle or 0.75 unit/kg body weight insulin as indicated. Liver gene expression was analyzed by real-time PCR after 3 hours. n = 4 per group. *P < 0.05; **P < 0.01. Values are shown as mean ± SEM.

Altered hepatic ER PC composition promotes lipogenesis in obesity. Enhanced hepatic lipogenesis and SREBP-1c pathway activity are hallmark features of obesity-linked insulin resistance. We therefore tested whether the composition of ER phospholipids was altered in *ob/ob* mice. ER was isolated from liver of WT or *ob/ob* mice and the enrichment of the resulting fractions was confirmed by Western blotting (Figure 6A). ER from *ob/ob* mice had elevated levels of a range of polyunsaturated PC species, particularly 18:0/18:2 PC, 18:1/18:2 PC, 18:0/20:4 PC, 18:1/20:4 PC, and 18:0/22:6 PC (Figure 6B). There was also a notable decrease in the abundance of saturated 16:0/18:0 PC. Interestingly, many of these same species were also altered in the fasting-refeeding studies described above. With the exception of decreased abundance of 16:0/18:2 PC, the overall trend of these changes was toward a decrease in PC acyl chain saturation in *ob/ob* mice. PE was far less abundant than PC in ER membranes, and with the exception of a decrease in 16:0/18:2 PE, only modest changes in acyl chain saturation were observed in *ob/ob* compared with WT mice (Supplemental Figure 5).

Since many of the species changed in our lipidomic analyses are known to be products of the LPCAT3 enzyme (25, 26), we proceeded to investigate the importance of LPCAT3 activity in determining the phospholipid profile of *ob/ob* ER. We found that expression of *Lpcat3* mRNA was higher in *ob/ob* compared with WT liver, suggesting that elevated LPCAT3 activity could be driving polyunsaturated PC incorporation into membranes in *ob/ob* mice (Figure 6C). Consistent with this hypothesis, knocking down LPCAT3 expression in *ob/ob* mouse liver with an adenoviral shRNA vector normalized the levels of these polyunsaturated PC species (Figure 6D). Indeed, the effects of *ob/ob* genotype and LPCAT3 knockdown were almost exactly reciprocal.

Inhibition of LPCAT3 blunts lipogenesis in obese mice. To further assess the relevance of LPCAT3 activity for lipogenesis in the setting of obesity and insulin resistance, we asked whether loss of LPCAT3 expression would inhibit SREBP-1c target gene expression in obese mice. Knockdown of LPCAT3 expression in liver by means of an adenoviral shRNA vector reduced mature SREBP-1c protein (Figure 7A) and lowered hepatic triglyceride levels (Figure 7B). Accordingly, LPCAT3 knockdown also reduced the expression of a battery of SREBP-1c target genes (Figure 7C) and reduced hepatic steatosis as assessed by histology (Figure 7D).

We reasoned that if LPCAT3 were an important driver of lipogenesis in obese mice, then increasing LPCAT3 activity should further increase the expression of SREBP-1c target genes. In support of this hypothesis, expression of LPCAT3 in obese mouse liver with an adenoviral vector further stimulated lipogenic program (Figure 8A). Finally, we tested whether increasing LPCAT3 expression could promote the lipogenic gene program in high-fat diet–fed mice. C57BL/6 mice were fed a western diet for 12 weeks

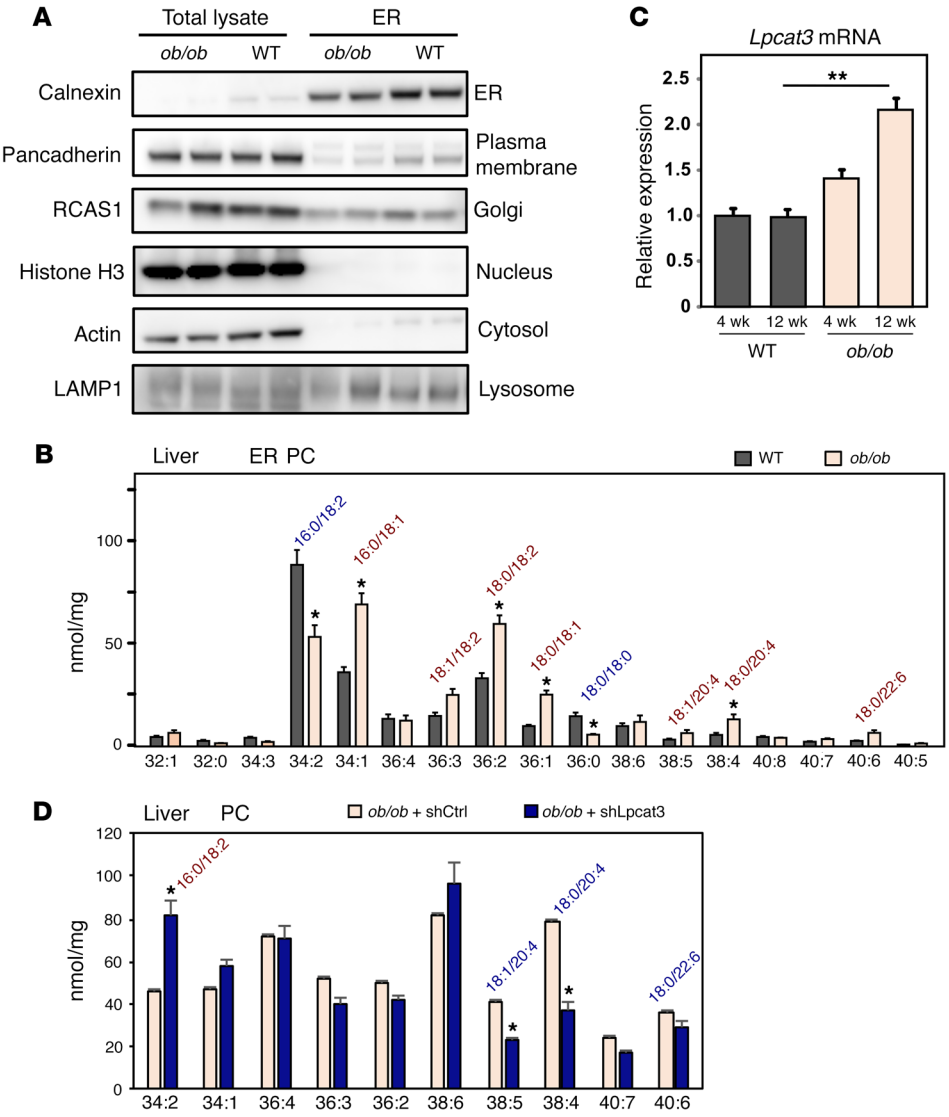

Figure 6. LPCAT3 mediates changes in ER phospholipid composition in obesity. (**A**) Validation of ER fractionation of mouse liver extracts by immunoblot analysis of subcellular markers. (**B**) ESI-MS/MS analysis of PC species in the ER fraction from C57BL/6 and *ob/ob* mouse liver. Indicated (*sn*-1/*sn*-2) molecular species were confirmed by product ion scanning for aliphatic composition. n = 6 per group. Statistical analysis was by Student's t test with correction for multiple comparisons using the Holm-Šidák method. $^*P < 0.05$. Values are shown as mean ± SEM. (**C**) *Lpcat3* expression in livers of C57BL/6 and *ob/ob* mice at 4 weeks and 12 weeks of age analyzed by real-time PCR. n = 5 per group. Statistical analysis was by 1-way ANOVA with Bonferroni's post hoc tests. $^{**}P < 0.01$. Values are shown as mean ± SEM. (**D**) ESI-MS/MS analysis of liver PC species from *ob/ob* mice transduced with adenoviral shCtrl or shLPCAT3 vectors for 7 days. Indicated (*sn*-1/*sn*-2) molecular species were confirmed by product ion scanning for aliphatic composition. n = 6 per group. Statistical analysis was by Student's t test with correction for multiple comparisons using the Holm-Šidák method. $^*P < 0.05$. Values are shown as mean ± SEM.

and then transduced for 7 days with GFP control or LPCAT3-expressing adenoviral vectors. Again, we observed elevated expression of SREBP-1c target genes in mice overexpressing LPCAT3 (Figure 8B). Collectively, these results demonstrate that LPCAT3 activity and ER phospholipid composition are important determinants of SREBP-1c activation and lipogenesis.

Discussion

The differential sensitivity of SREBP-1c and SREBP2 cleavage to sterols in vivo has suggested that the abundance of another cellular lipid might preferentially affect SREBP-1c activation. Here, we have shown that the ER abundance of polyunsaturated PC is closely linked with hepatic lipogenesis in both physiological and pathological contexts. We further showed that LPCAT3-dependent incorporation of polyunsaturated fatty acids into PC is a determinant of lipogenic gene expression during feeding and in the setting of obesity-linked insulin resistance. These observations identify a mechanism whereby dynamic changes in ER phospholipid composition can selectively modulate SREBP-1c processing and lipogenesis.

Our results support a regulatory mechanism in which LPCAT3-mediated phospholipid remodeling alters the abundance of specific PC species in the ER membrane. Importantly, the effect of membrane fatty acyl chain composition on SREBP-1c processing is SCAP dependent and therefore presumably involves the transport of SREBP-1c from ER to Golgi. The exact mechanism by which ER membrane phospholipid composition regulates SREBP-1c processing is not yet clear; however, our results support a biophysical model in which the flexible polyunsaturated fatty acyl chains in the local environment of the SREBP-1c/SCAP/Insig complex increase membrane dynamics and facilitate release of the SREBP-1c/SCAP complex from the ER. In line with this model, we previously demonstrated that loss of LPCAT3 expression in hepatocytes reduces the fluidity of intracellular membranes, but does not perturb ER or Golgi structure (19).

It seems most likely that the previously described inhibitory effects of free polyunsaturated fatty acids on SREBP-1 activity occur through LPCAT3-independent mechanisms (13, 27). We did not observe accumulation of linoleate or arachidonate in the setting of chronic LPCAT3 deficiency, suggesting that these sub-

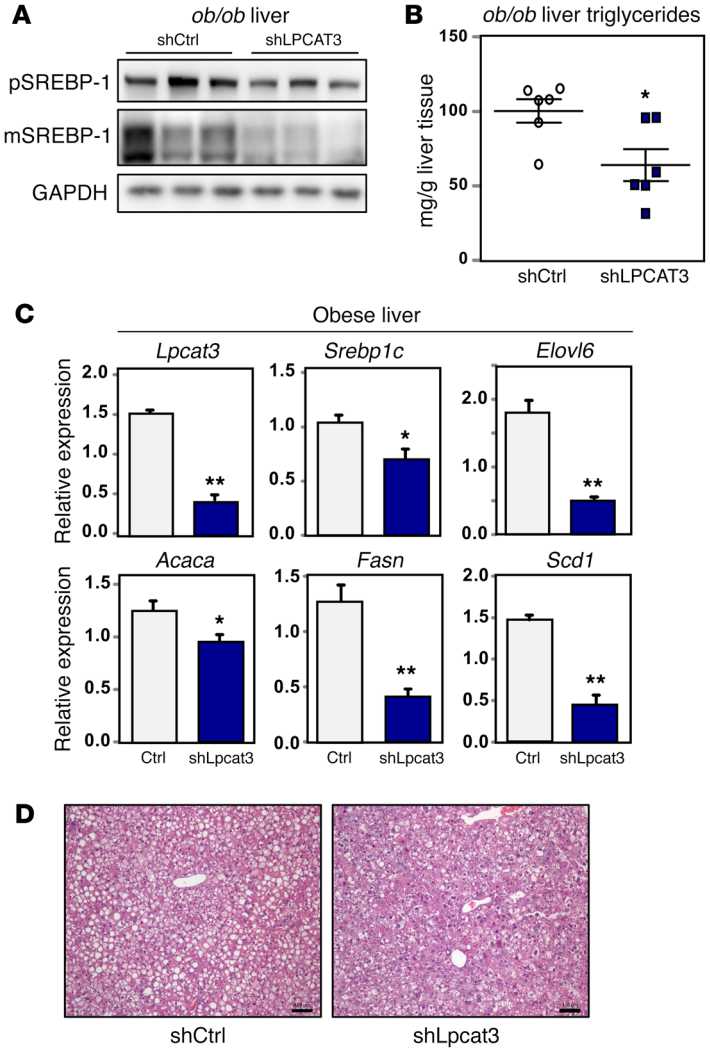

Figure 7. LPCAT3 promotes SREBP-1c processing and hepatic lipogenesis in obesity. (**A**) Levels of precleaved SREBP-1 and mature SREBP-1 were analyzed in livers from *ob/ob* mice transduced with adenoviral shRNA targeting LPCAT3 (shLPCAT3) or control for 7 days. GAPDH was used as internal loading control. (**B**) Hepatic triglyceride levels of mice used for **A**. (**C**) Liver gene expression was determined by real-time PCR in mice used for **A**. $n = 6$ per group. Statistical analysis was by 1-way ANOVA with Bonferroni's post hoc tests. (**D**) H&E staining of liver sections from *ob/ob* mice transduced with adenoviral vectors expressing shRNA targeting LPCAT3 (shLPCAT3) or control LPCAT for 7 days. Original magnification: ×100. $^*P < 0.05$; $^{**}P < 0.01$. Values are shown as mean ± SEM.

strates are channeled into alternative lipids such as triglycerides. Our findings are also compatible with previously proposed parallel pathways for modulation of SREBP-1c activity or processing, such as may occur with activation of mTOR (28).

How LPCAT3 activity is regulated in various physiological and pathological contexts remains to be fully clarified. Our data suggest that LXR-dependent induction of LPCAT3 facilitates the lipogenic response to a sterol-rich diet. In addition, we found that *Lpcat3* mRNA increases in the setting of obesity and that increased LPCAT3 activity contributes to the increased abundance of polyunsaturated PC species in *ob/ob* liver ER. Interestingly, however, in the setting of feeding, we observed increased ER polyunsaturated PC abundance in the absence of changes in *Lpcat3* mRNA. This observation suggests that, while LPCAT3 is required for efficient incorporation of polyunsaturated fatty acids into PC during feeding, the change in product abundance in this setting may be driven by increased substrate availability rather than a change in enzyme activity. Thus, the change in ER phospholipid composition may serve as an auxiliary signal of the fed state that facilitates an increase in lipid synthesis in response to nutrient availability.

Stimulation of *Srebf1c* transcription is an important contributor to the lipogenic effects of LXR agonists (16, 17). The current finding that LXRs selectively promote SREBP-1c versus SREBP-2 processing adds another layer of regulatory complexity to the control of hepatic lipogenesis. We previously reported that LPCAT3-dependent polyunsaturated PC production promotes hepatic triglyceride secretion. Coupled with prior observations, the present data suggest that LPCAT3-dependent modulation of membrane phospholipid composition is a common mechanism by which LXRs integrate hepatic lipid synthesis and secretion.

Our study also links aberrant phospholipid metabolism to the excessive lipogenesis characteristic of obesity-linked insulin resistance. Although hyperinsulinemia is a major driver of SREBP-1c hyperactivation (29), our data suggest that increased membrane polyunsaturated PC abundance is also a contributor. Interestingly, altered membrane composition has been observed in patients with metabolic liver disease (30). We speculate that the increase in polyunsaturated PC in obesity, especially ω-6 fatty acyl PC, may be due to a combination of excessive intake of these essential fatty acids and increased LPCAT3 expression. Our observation that blocking the incorporation of polyunsaturated PC into membranes in *ob/ob* mice reduces lipogenesis and lowers hepatic triglyceride levels raises the possibility that pharmacologic LPCAT3 inhibition may be of potential therapeutic benefit in the setting of fatty liver disease.

In conclusion, our results highlight the dynamism of cellular membranes and reveal the importance of rapid membrane acyl chain remodeling in the setting of metabolic flux. Together with prior work (19, 31), these findings contribute to an emerging view of dynamic manipulation of membrane acyl chain composition as a regulatory strategy in the control of metabolic pathways.

Methods

Gene expression. Total RNA was isolated from cells and tissues with TRIzol (Invitrogen). cDNA was synthesized, and gene expression was quantified by real-time PCR with SYBR Green (Diagenode) and an Applied Biosystems Quantstudio 6 Flex. Gene expression levels were normalized to 36B4 or GAPDH.

Cell culture. Primary hepatocytes were isolated from *Lpcat3*$^{fl/fl}$, *Lpcat3*$^{fl/fl}$*; albumin-Cre* mice. Briefly, we cannulated the inferior vena cava of anesthetized mice and perfused the liver with 37°C liver perfusion medium (Thermo Fisher Scientific) for 5 minutes, then with 40 μg/ml 37°C Liberase TM in 10 mM HEPES-buffered William E medi-

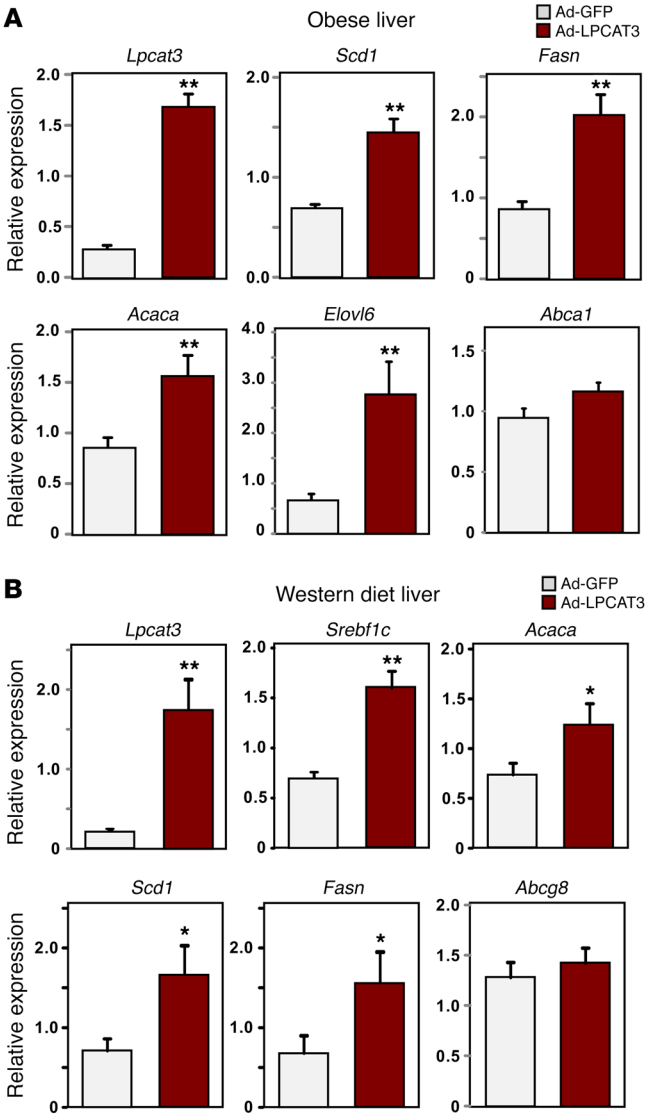

Figure 8. Enhances LPCAT3 activity drives hepatic lipogenesis. (**A**) *ob/ob* mice were transduced with adenoviral vectors expressing LPCAT3 or GFP for 7 days. $n = 5$ per group. (**B**) C57BL/6 mice were fed a western diet for 12 weeks and transduced with adenoviral vectors expressing LPCAT3 or GFP for 7 days. $n = 5$ per group. Gene expression was analyzed by real-time PCR. Statistical analysis was by Student's t test. $^*P < 0.05$; $^{**}P < 0.01$. Values are shown as mean ± SEM.

um for another 5 minutes. Perfused and digested liver was removed and placed in hepatocyte wash medium (Thermo Fisher Scientific), and cells were dispersed. We filtered the resulting cell suspension through a 100-μm cell strainer and washed it 3 times with hepatocyte wash medium. Live cells were counted using trypan blue staining. Primary hepatocytes were used only when the viability was above 85%. 1×10^6 live cells were seeded per well of 6-well collagen I–coated Biocoat dishes in William E medium supplemented with 10 mM HEPES, 1% penicillin and streptomycin, 5% FBS (Omega Scientific Inc.), 100 nM insulin (Thermo Fisher Scientific), and 1 μM dexamethasone (Sigma-Aldrich). After 3 to 4 hours, cells were washed once with 2 ml PBS and cultured in William E medium supplemented with primary hepatocyte maintenance supplements (Thermo Fisher Scientific). For adenoviral infections, VQAd-CMV Cre/eGFP and VQAd-Empty eGFP were purchased from Viraquest and used at an MOI of 10. HSV–SREBP-1c–expressing adenovirus was generated by cloning mouse SREBP-1c with 2 tandem copies of the HSV epitope tag (QPELAPEDPED) at the N terminus into the pAd/CMV/V5-DEST vector (Thermo Fisher Scientific) using the Gateway Cloning System (Thermo Fisher Scientific). Adenovirus was generated per the manufacturer's instructions. pCMV-sport6 vector expressing human truncated nuclear SREBP-1c form was a gift from Elizabeth J. Tarling (UCLA, Los Angeles, CA, USA). On day 1, 293T cells were cultured in 10% serum DMEM medium and transfected with 400 ng pCMV-sport6-nSREBP-1c. After 6 hours, cells were changed to fresh medium with 10% serum with LXR agonist or vehicle. On day 2, cells were changed to DMEM with 1% serum for 12 hours and harvested in RIPA buffer.

Mice. *Lpcat3*$^{fl/fl}$, *Lpcat3*$^{fl/fl}$*; albumin-Cre* mice have been described (19). Male C57BL/6 and *ob/ob* mice (8 to 12 weeks old) were acquired from the Jackson Laboratory. *Scap*$^{fl/fl}$ mice were previously described (10). All mice were housed under pathogen-free conditions in a temperature-controlled room with a 12-hour light/12-hour dark cycle. Mice were fed a chow diet, a western diet (Research Diets catalog D12079B), a high-fat diet (Research Diets catalog D12492), or a high-carbohydrate diet (Research Diets catalog D07042201). For RNA and whole liver protein analysis, liver tissues were collected and frozen in liquid nitrogen and stored at −80°C. In the fasting and refeeding experiments, the fasted group was fasted 12 hours, and the refed group was fasted for 12 hours and then refed a high-carbohydrate diet (Research Diets catalog D07042201) or a high-fat diet (Research Diets catalog D12492) for 12 hours prior to study. The starting times for the experiments were staggered so that all mice were sacrificed at the same time, which was at the end of the dark cycle. For the ligand gavage experiments, mice were gavaged with 40 mg/kg body weight GW3965 once per day for 3 days in the morning. Liver tissues were harvested 3 to 4 hours after the last gavage. For adenoviral infections, 8- to 10-week-old male mice were injected with 2×10^9 or 3×10^9 PFU by the tail vein. Mice were sacrificed 6 to 9 days later following a 6-hour fast. For testing insulin-induced lipogenic response in mice, mice were infected with indicated adenovirus for 7 days. On the day of the experiment, mice were fasted for 2 hours prior to the intraperitoneal injection of 0.75 unit/kg body weight of insulin or vehicle. Liver tissues were harvested 3 hours after insulin injection. The LPCAT3 adenoviral vectors used in these studies were described previously (22).

ER fractionation from mouse liver. ER membranes were prepared following the method of Croze and Morré (32), with the modification that only the supernatant of the initial centrifugation of homogenate at 5,000 *g* was used for the following ER purification. ER membrane was resuspended in saline for lipidomic analysis.

Protein analysis. Whole cells and tissue lysates were prepared by homogenization in RIPA buffer (50 mM Tris–HCl, pH 7.4, 150 mM NaCl, 1% NP-40, 0.5% sodium deoxycholate, 0.1% SDS) supplemented with protease inhibitors (Roche Molecular Biochemicals). Lysates were cleared by centrifugation. Membrane and nuclear preparations of cells were performed as described (12). Briefly, cells were collected in buffer A (10 mM Hepes-KOH at pH 7.4, 10 mM KCl, 1.5 mM $MgCl_2$, 0.5 mM sodium EDTA, 0.5 mM sodium EGTA, and 100 mM NaCl), passed through 25-gauge needles 20 times, and spun at 1,000 *g* for 10 minutes at 4°C. The pellets were resuspended

in buffer B (10 mM Hepes-KOH at pH 7.4, 0.42 M NaCl, 2.5% [v/v] glycerol, 1.5 mM $MgCl_2$, 0.5 mM sodium EDTA, 0.5 mM EGTA, 1 mM dithiothreitol, and the protease inhibitors), rotated 30 minutes at 4°C, and centrifuged at 100,000 *g* for 30 minutes at 4°C. The resulting supernatant was collected as the nuclear fraction. The supernatant from the 1,000 *g* spin was centrifuged at 100,000 *g* for 30 minutes at 4°C, and the resulting pellet was lysed in RIPA buffer with protease inhibitors as membrane fraction. Membrane and nuclear preparation from liver were performed as described (33). Briefly, liver was perfused with saline and homogenized in homogenization buffer (10 mM HEPES, pH 7.6, 25 mM KCl, 1 mM sodium EDTA, 2 M sucrose, 10% glycerol, 0.15 mM spermine, 2 mM spermidine) with protease inhibitors. The liver lysate was layered over the homogenization buffer and centrifuged at 85,000 *g* for 1 hour at 4°C. Pellets were lysed by nuclear lysis buffer (50 mm Tris, pH 7.6, 0.5 M NaCl) with protease inhibitors, rotated 30 minutes at 4°C, and centrifuged at 100,000 *g* for 30 minutes at 4°C. The resulting supernatant contained the nuclear fraction. For liver membrane, liver tissues were homogenized and centrifuged at 1000 *g* at 4°C for 5 minutes. Then the resulting 1000 *g* supernatant was centrifuged again at 100,000 *g* at 4°C for 30 minutes. Pellets were lysed in RIPA buffer as membrane fraction. Protein lysates were then mixed with NuPAGE LDS Sample Buffer, size-fractionated on 4%–12% Bis-Tris Gels (Invitrogen), transferred to hybond ECL membrane (GE Healthcare), and incubated with the indicated primary antibodies: anti-HSV (Millipore, 69171), anti-HMGB1 (Abcam, ab18256), anti–SREBP-1 (2A4, gift from Timothy Osborne, Sanford Burnham Prebys Medical Discovery Institute, Orlando, FL, USA), anti–SREBP-2 (gift from Timothy Osborne), Calnexin (Abcam, ab10286), pan-cadherin (Santa Cruz Biotechnology, sc-59876), RCAS1 (Cell Signaling Technology, 12290P), histone H3 (Abcam, AB4729), actin (Sigma-Aldrich, A2066), LSMP1 (Abcam, ab24170), and GAPDH (Genetex, GTX627408). Primary antibody binding was detected with suitable secondary antibody and visualized with chemiluminescence (ECL, Amersham Pharmacia Biotech). The immunoblotting results were quantified by ImageJ (NIH).

Liposomes. All the phospholipids used in the study were purchased from Avanti Polar Lipids. 1 μmol phospholipids dissolved in chloroform were evaporated under a stream of nitrogen gas and thoroughly dried by rotary vacuum dryer. Dry phospholipids were then hydrated in 1 ml saline at a temperature above its transition temperature and vortexed vigorously. The phospholipid solution was passed through 50–80 nm PCTE membrane filters (Sterlitech) 10 times to make small unilaminar liposomes. ER-targeting liposomes were generated as described (23) and were composed of PC/PE/PS/PI at a molar ratio of 1.5:1.5:1:1. The PE and PI components were derived from bovine liver and the PS component from porcine brain. The PC component was contributed by defined species as indicated. To label the liposome for imaging, 10 nmol β-BODIPY FL C12-HPC-1-hexadecanoyl-sn-glycero-3-phosphocholine (Thermo Fisher Scientific) was added to the 1 μmol phospholipid mix.

Liposome uptake assay. Primary hepatocytes were harvested and treated with fluorescent-labeled ER-targeting liposomes as described above. After 3 hours of treatment, cells were washed with PBS 3 times and lysed with RIPA buffer. Cell lysate was cleared by spinning at 12,000 *g* for 5 minutes at 4°C. Fluorescence of lysates was measured by CLARIOstar plate reader (BMG Labtech), with background subtracted and normalized to protein concentration.

Imaging. For imaging studies, cells were incubated with labeled ER-targeting liposome at 30 μM for 15 minutes, washed once with PBS, and incubated in fresh culture medium without liposome for 1 hour. For the last 15 minutes, ER-Tracker Blue-White DPX (Thermo Fisher Scientific) was added to the medium to stain ER following the manufacturer's instructions. Cells were then fixed with 4% paraformaldehyde (Thermo Fisher Scientific), mounted with ProLong Diamond Antifade Mountant, and imaged with a Carl Zeiss Laser Scanning System LSM 510 META confocal microscope.

Lipid analyses. Liver tissue and ER fraction were snap-frozen at the temperature of liquid nitrogen. To extract lipids, liver tissue and ER fraction were subsequently subjected to a modified Bligh-Dyer lipid extraction (34) in the presence of lipid class internal standards including 1-0-heptadecanoyl-sn-glycero-3-phosphocholine, 1,2-dieicosanoyl-sn-glycero-3-phosphocholine, and 1,2-ditetradecanoyl-sn-glycero-3-phosphoethanolamine (35). Lipid extracts were diluted in methanol/chloroform (4/1, v/v), and molecular species were quantified using ESI-MS on a triple-quadrupole instrument (Thermo Fisher Quantum Ultra) employing shotgun lipidomics methodologies (36). PC molecular species were quantified as chlorinated adducts in the negative ion mode using neutral loss scanning for 50 amu (collision energy = 24 eV). PE molecular species were first converted to fMOC derivatives and then quantified in the negative ion mode using neutral loss scanning for 222.2 amu (collision energy = 30 eV). Individual molecular species were quantified by comparing the ion intensities of the individual molecular species to that of the lipid class internal standard with additional corrections for type I and type II 13C isotope effects (36). Where XX:YY/XX:YY species are provided in the figures, each molecular species was confirmed by concomitant analyses of samples using product ion scanning for individual fatty acid constituents, including palmitoleic, palmitate, linoleate, oleate, stearate, arachidonate, and docosohexadecanoate (product ion scans in *m/z* of 253.2, 255.2, 279.3, 281.3, 283.3, 303.4, and 327.4, respectively, at a collision energy + 35 eV).

Major PC species identified in ER membrane were subjected to further analyses to provide information for the regioisomers of acyl chains. The sodiated adducts of major species were subjected to CAD analyses, which yield regioisomer information by determining the ratio of the fragment ions from the loss of trimethylamine and the fatty acid of the parent molecular ion (37). This technique has been shown to provide over 2- to 4-fold greater ion intensity for the loss of the fatty acyl chain from the *sn*-1 position.

Author contributions

XR, BW, and ENDP performed experiments. XR, BW, DAF, and PT designed experiments and interpreted data. TQDAV provided essential reagents and interpreted data. XR and PT wrote the paper.

Acknowledgments

We thank T. Osborne for SREBP antibodies, J. Gao for imaging support, and E. Tarling for the nuclear SREBP-1c plasmid. This work was supported by NIH grants HL030568 and DK063491.

Address correspondence to: Peter Tontonoz, Department of Pathology and Laboratory Medicine, 675 Charles Young Drive, University of California, Los Angeles, California 90095, USA. Phone: 310.206.4546; Email: ptontonoz@mednet.ucla.edu.

1. Hua X, Nohturfft A, Goldstein JL, Brown MS. Sterol resistance in CHO cells traced to point mutation in SREBP cleavage-activating protein. *Cell*. 1996;87(3):415–426.
2. Yang T, et al. Crucial step in cholesterol homeostasis: sterols promote binding of SCAP to INSIG-1, a membrane protein that facilitates retention of SREBPs in ER. *Cell*. 2002;110(4):489–500.
3. Yabe D, Brown MS, Goldstein JL. Insig-2, a second endoplasmic reticulum protein that binds SCAP and blocks export of sterol regulatory element-binding proteins. *Proc Natl Acad Sci U S A*. 2002;99(20):12753–12758.
4. Sakai J, et al. Molecular identification of the sterol-regulated luminal protease that cleaves SREBPs and controls lipid composition of animal cells. *Mol Cell*. 1998;2(4):505–514.
5. Rawson RB, et al. Complementation cloning of S2P, a gene encoding a putative metalloprotease required for intramembrane cleavage of SREBPs. *Mol Cell*. 1997;1(1):47–57.
6. Horton JD, Bashmakov Y, Shimomura I, Shimano H. Regulation of sterol regulatory element binding proteins in livers of fasted and refed mice. *Proc Natl Acad Sci U S A*. 1998;95(11):5987–5992.
7. Shimomura I, Bashmakov Y, Horton JD. Increased levels of nuclear SREBP-1c associated with fatty livers in two mouse models of diabetes mellitus. *J Biol Chem*. 1999;274(42):30028–30032.
8. Shimomura I, Hammer RE, Ikemoto S, Brown MS, Goldstein JL. Leptin reverses insulin resistance and diabetes mellitus in mice with congenital lipodystrophy. *Nature*. 1999;401(6748):73–76.
9. Radhakrishnan A, Goldstein JL, McDonald JG, Brown MS. Switch-like control of SREBP-2 transport triggered by small changes in ER cholesterol: a delicate balance. *Cell Metab*. 2008;8(6):512–521.
10. Matsuda M, et al. SREBP cleavage-activating protein (SCAP) is required for increased lipid synthesis in liver induced by cholesterol deprivation and insulin elevation. *Genes Dev*. 2001;15(10):1206–1216.
11. Kalaany NY, et al. LXRs regulate the balance between fat storage and oxidation. *Cell Metab*. 2005;1(4):231–244.
12. Hua X, Sakai J, Brown MS, Goldstein JL. Regulated cleavage of sterol regulatory element binding proteins requires sequences on both sides of the endoplasmic reticulum membrane. *J Biol Chem*. 1996;271(17):10379–10384.
13. Ou J, et al. Unsaturated fatty acids inhibit transcription of the sterol regulatory element-binding protein-1c (SREBP-1c) gene by antagonizing ligand-dependent activation of the LXR. *Proc Natl Acad Sci U S A*. 2001;98(11):6027–6032.
14. Dobrosotskaya IY, Seegmiller AC, Brown MS, Goldstein JL, Rawson RB. Regulation of SREBP processing and membrane lipid production by phospholipids in Drosophila. *Science*. 2002;296(5569):879–883.
15. Walker AK, et al. A conserved SREBP-1/phosphatidylcholine feedback circuit regulates lipogenesis in metazoans. *Cell*. 2011;147(4):840–852.
16. Repa JJ, et al. Regulation of mouse sterol regulatory element-binding protein-1c gene (SREBP-1c) by oxysterol receptors, LXRalpha and LXRbeta. *Genes Dev*. 2000;14(22):2819–2830.
17. DeBose-Boyd RA, Ou J, Goldstein JL, Brown MS. Expression of sterol regulatory element-binding protein 1c (SREBP-1c) mRNA in rat hepatoma cells requires endogenous LXR ligands. *Proc Natl Acad Sci U S A*. 2001;98(4):1477–1482.
18. Okazaki H, Goldstein JL, Brown MS, Liang G. LXR-SREBP-1c-phospholipid transfer protein axis controls very low density lipoprotein (VLDL) particle size. *J Biol Chem*. 2010;285(9):6801–6810.
19. Rong X, et al. Lpcat3-dependent production of arachidonoyl phospholipids is a key determinant of triglyceride secretion. *Elife*. 2015;4:e06557.
20. Beaven SW, et al. Reciprocal regulation of hepatic and adipose lipogenesis by liver X receptors in obesity and insulin resistance. *Cell Metab*. 2013;18(1):106–117.
21. Liang G, Yang J, Horton JD, Hammer RE, Goldstein JL, Brown MS. Diminished hepatic response to fasting/refeeding and liver X receptor agonists in mice with selective deficiency of sterol regulatory element-binding protein-1c. *J Biol Chem*. 2002;277(11):9520–9528.
22. Rong X, et al. LXRs regulate ER stress and inflammation through dynamic modulation of membrane phospholipid composition. *Cell Metab*. 2013;18(5):685–697.
23. Pollock S, et al. Uptake and trafficking of liposomes to the endoplasmic reticulum. *FASEB J*. 2010;24(6):1866–1878.
24. DeBose-Boyd RA, Brown MS, Li WP, Nohturfft A, Goldstein JL, Espenshade PJ. Transport-dependent proteolysis of SREBP: relocation of site-1 protease from Golgi to ER obviates the need for SREBP transport to Golgi. *Cell*. 1999;99(7):703–712.
25. Hishikawa D, Shindou H, Kobayashi S, Nakanishi H, Taguchi R, Shimizu T. Discovery of a lysophospholipid acyltransferase family essential for membrane asymmetry and diversity. *Proc Natl Acad Sci U S A*. 2008;105(8):2830–2835.
26. Zhao Y, et al. Identification and characterization of a major liver lysophosphatidylcholine acyltransferase. *J Biol Chem*. 2008;283(13):8258–8265.
27. Hannah VC, Ou J, Luong A, Goldstein JL, Brown MS. Unsaturated fatty acids down-regulate srebp isoforms 1a and 1c by two mechanisms in HEK-293 cells. *J Biol Chem*. 2001;276(6):4365–4372.
28. Peterson TR, et al. mTOR complex 1 regulates lipin 1 localization to control the SREBP pathway. *Cell*. 2011;146(3):408–420.
29. Farese RV, Zechner R, Newgard CB, Walther TC. The problem of establishing relationships between hepatic steatosis and hepatic insulin resistance. *Cell Metab*. 2012;15(5):570–573.
30. Puri P, et al. A lipidomic analysis of nonalcoholic fatty liver disease. *Hepatology*. 2007;46(4):1081–1090.
31. Wang B, et al. Intestinal phospholipid remodeling is required for dietary-lipid uptake and survival on a high-fat diet. *Cell Metab*. 2016;23(3):492–504.
32. Croze EM, Morré DJ. Isolation of plasma membrane, Golgi apparatus, and endoplasmic reticulum fractions from single homogenates of mouse liver. *J Cell Physiol*. 1984;119(1):46–57.
33. Sheng Z, Otani H, Brown MS, Goldstein JL. Independent regulation of sterol regulatory element-binding proteins 1 and 2 in hamster liver. *Proc Natl Acad Sci U S A*. 1995;92(4):935–938.
34. Bligh EG, Dyer WJ. A rapid method of total lipid extraction and purification. *Can J Biochem Physiol*. 1959;37(8):911–917.
35. Demarco VG, et al. Obesity-related alterations in cardiac lipid profile and nondipping blood pressure pattern during transition to diastolic dysfunction in male db/db mice. *Endocrinology*. 2013;154(1):159–171.
36. Han X, Gross RW. Shotgun lipidomics: electrospray ionization mass spectrometric analysis and quantitation of cellular lipidomes directly from crude extracts of biological samples. *Mass Spectrom Rev*. 2005;24(3):367–412.
37. Yang K, Zhao Z, Gross RW, Han X. Systematic analysis of choline-containing phospholipids using multi-dimensional mass spectrometry-based shotgun lipidomics. *J Chromatogr B Analyt Technol Biomed Life Sci*. 2009;877(26):2924–2936.